

ORIGINAL ARTICLE

# Volumetric changes of the enteric nervous system under physiological and pathological conditions measured using x-ray phase-contrast tomography

Niccolò Peruzzi,\* Marina Eckermann,<sup>†,‡,§</sup> Jasper Frohn,<sup>‡,§</sup> Tim Salditt,<sup>‡,§</sup> Bodil Ohlsson<sup>¶,||</sup> and Martin Bech<sup>\*,\*\*,\*\*\*</sup> 

\*Medical Radiation Physics, Department of Clinical Sciences Lund, <sup>¶</sup>Department of Clinical Sciences Malmö, Lund University, <sup>\*\*</sup>LINXS Institute of advanced Neutron and X-ray Science (LINXS), Lund, <sup>||</sup>Department of Internal Medicine, Skåne University Hospital, Malmö, Sweden, <sup>†</sup>ESRF, The European Synchrotron, Grenoble, France, <sup>‡</sup>Institute for X-Ray Physics, University of Göttingen and <sup>§</sup>Cluster of Excellence “Multiscale Bioimaging: from Molecular Machines to Networks of Excitable Cells” (MBExC), University of Göttingen, Göttingen, Germany

## Key words

dysmotility, enteric nervous system, histopathology, three-dimensional, volumetric measurements, x-ray phase-contrast tomography.

Accepted for publication 1 September 2024.

## Correspondence

Professor Bodil Ohlsson, Jan Waldenströms Gata 15, Floor 5, 205 02 Malmö, Sweden. Email: [bodil.ohlsson@med.lu.se](mailto:bodil.ohlsson@med.lu.se)

Bodil Ohlsson and Martin Bech contributed equally to this work.

**Declaration of conflict of interest:** The authors confirm that there are no conflicts of interest.

**Author contribution:** Bodil Ohlsson and Martin Bech contributed to the conceptualization. All authors contributed to the methodology and writing—review and editing. Niccolò Peruzzi, Marina Eckermann, Jasper Frohn, Bodil Ohlsson, Martin Bech contributed to the investigation. Niccolò Peruzzi contributed to the data curation and visualization. Niccolò Peruzzi and Bodil Ohlsson were involved in the Writing—original draft preparation.

**Financial support:** Bodil Ohlsson received grants from the Development Foundation of Region Skåne, Foundation of Skåne University Hospital, and Ingrid & Sverker Persson's Foundation. The funders had no role in study design, data collection and analysis, decisions to publish, or preparation of the manuscript. Martin Bech acknowledges funding from the Swedish Research Council (grant number 2022-04192).

**Funding support:** Vetenskapsrådet 2022-04192; Ingrid & Sverker Perssons Foundation; Region Skåne; Skåne University Hospital

## Introduction

The enteric nervous system (ENS), situated along the gastrointestinal tract, is built up mainly of neurons assembled into ganglia and interconnected through nerve trunks.<sup>1</sup> The ganglia of the

## Abstract

**Background and Aim:** Full-thickness biopsies of the intestinal wall may be used to study and assess damage to the neurons of the enteric nervous system (ENS), that is, enteric neuropathy. The ENS is difficult to examine due to its localization deep in the intestinal wall and its organization with several connections in diverging directions. Histological sections used in clinical practice only visualize the sample in a two-dimensional way. X-ray phase-contrast micro-computed tomography (PC- $\mu$ CT) has shown potential to assess the cross-sectional thickness and volume of the ENS in three dimensions (3D). The aim of this study was to explore the potential of PC- $\mu$ CT to evaluate its use to determine the size of the ENS.

**Methods:** Full-thickness biopsies of ileum obtained during surgery from five controls and six patients clinically diagnosed with enteric neuropathy and dysmotility were included. Punch biopsies of 1 mm in diameter and 1 cm in length, from an area containing myenteric plexus, were extracted from paraffin blocks, and scanned with synchrotron-based PC- $\mu$ CT without any staining.

**Results:** The microscopic volumetric structure of the neural tissue (consisting of both ganglia and fascicles) could be determined in all samples. The ratio of neural tissue volume/total tissue volume was higher in controls than in patients with enteric neuropathy ( $P = 0.013$ ). The patient with the longest disease duration had the lowest ratio.

**Conclusion:** The assessment of neural tissue can be performed in an objective, standardized way, to ensure reproducibility and comparison under physiological and pathological conditions. Further evaluation is needed to examine the role of this method in the diagnosis of enteric neuropathy.

ENS are divided into the myenteric plexus located between muscle layers, and submucosal plexus located in the submucosa, in the small and large intestine. Damage to the ENS may lead to gastrointestinal dysmotility, one of the most severe being chronic

intestinal pseudo-obstruction (CIPO).<sup>2–4</sup> These disorders have different etiologies, the most common being diabetes, neurological diseases, rheumatological diseases, drugs, genetic variants, or idiopathic conditions.<sup>5</sup> Not only neuropathy, but also myopathy is present, either as a primary damage or secondary to the neuropathy.<sup>3</sup> Enteric neuropathy is seldom studied, and there are few centers available for evaluation of gastrointestinal motility. A newly developed magnetic resonance imaging (MRI)-based quantification of the alimentary function can identify dysmotility secondary to enteric neuropathy and classify into different categories through machine learning.<sup>6</sup>

Due to the localization, there are difficulties to access full-thickness samples of ENS and disadvantages in the use of histopathological examination with immunostaining of tissue samples, as the technique is a time-consuming work in sections of 3–5  $\mu\text{m}$ , whereas a neuron has the size of 15–40  $\mu\text{m}$ .<sup>3,7–9</sup> Thus, immunostaining and two-dimensional (2D) evaluation are of limited use to evaluate the volume of ENS to assess atrophy/hypertrophy of the ENS. We have recently proposed the use of x-ray phase-contrast micro-computed tomography (PC- $\mu\text{CT}$ ) to study the volume and structure of the ENS in a three-dimensional (3D) way.<sup>10</sup> The neurons and structure of the ENS are visible by this method without the need of any prior staining. Depending on the experimental configuration, different levels of magnification are possible. Levels may range from overview scans of full 1-mm punch biopsies, from which quantitative evaluations of the structural organization of the ENS could be extracted,<sup>10</sup> to high-resolution scans that could be used for more qualitative histopathological examination for description of neuropathy.<sup>10,11</sup> However, the high-resolution images are time-consuming in acquisition and evaluation time, pointing to their use mostly for highly selected cases. Our proposition is that 3D analysis of overview PC- $\mu\text{CT}$  scans in the future could be used in the daily clinical practice to evaluate the ENS by quantifying its cross-sectional thickness and volume, and thereby assess the degree of damage.

The aim of the present study was to further explore the potential of PC- $\mu\text{CT}$  in assessment of the size and structure of the ENS by increasing the sample number, to assess reproducibility and significance, and significantly reducing the scan time by performing the measurements at a synchrotron facility, with scan times cut down to a few minutes per sample. To this end, we have collected a cohort of patients with severe gastrointestinal dysmotility, which has already been described regarding clinical findings and histopathological examinations.<sup>9</sup>

## Methods

**Tissue samples.** Consecutive patients with severe gastrointestinal pain and dysmotility and subjected to laparoscopic full-thickness biopsy at the Departments of Surgery or Gastroenterology, Skåne University Hospital, Malmö, between 1998 and 2009, were retrospectively identified from September 2009 to April 2010 in a previous study.<sup>9</sup> Gastrointestinal investigations had been performed with esophageal manometry, gastric emptying scintigraphy, antroduodenojunal manometry, and/or colonic transit time after exclusion of organic disease. The patients had received the diagnosis CIPO when they fulfilled the three criteria: a medical history compatible with pseudo-

obstruction, documented events or chronic signs mimicking mechanical obstruction (bowel dilatation and/or air/fluid levels), and absence of mechanical obstruction or other organic cause for these symptoms and findings.<sup>2,4</sup> Patients with documented abnormal intestinal contractile activity, but no signs of mechanical obstruction and absence of any medication that could lead to the motor abnormalities, were classified as idiopathic gastrointestinal dysmotility when no systemic disease could explain the dysfunction.<sup>2–4</sup>

A standardized laparoscopy-assisted technique for small intestinal full-thickness biopsies and preparation of the biopsies was used, where full-thickness slices were cut perpendicular to each other and embedded in paraffin.<sup>8,9</sup> The histopathological examination performed for clinical use was obtained from the medical records, and not further repeated in the current study. Clinical and histopathological data are published in a separate publication.<sup>9</sup> One patient suffered from CIPO developed secondary to a drug use, one had diabetes with autonomic neuropathy, one had dysmotility secondary to Ehlers–Danlos syndrome, and the other three patients had idiopathic dysmotility without known etiology. A summary is presented in Table 1.

Ileum samples from the healthy resection region of four men, 45, 54, 61, and 82 years old, and one woman 85 years old, who had undergone surgery due to malignancy in the small and large intestine, were used as controls in the present PC- $\mu\text{CT}$  study.

After identification of 20 available paraffin blocks from patients representing ileum, a 4- $\mu\text{m}$ -thick slice was sectioned from the top of each block, stained with HE, and studied under the light microscope. The histopathological diagnoses and various stains, such as CD117 for interstitial cells of Cajal (ICC), CD34 for telocytes, S100 for Schwann cells, periodic acid-Schiff (PAS) with or without diastase (PAS-D) for carbohydrates or their compounds (e.g. glycogen and mucin), and p62 for sequestosome, were obtained from the medical records.<sup>11,12</sup> Examples of histological findings are displayed in Figure 1.

Ileum samples from six patients and five controls were selected for PC- $\mu\text{CT}$  as they contained enough tissue with representative parts to evaluate the ENS. A biopsy punch of 1 mm diameter centered on the ENS was taken from the paraffin blocks and placed into a Kapton<sup>®</sup> tube (Paramount, South Bend, Indiana, USA) for mounting in the subsequent tomographic investigation.<sup>10,13</sup> Two biopsies of different regions were taken from one control with a large resection. A detailed description of the histopathological findings in conventional light microscopy together with high-resolution PC- $\mu\text{CT}$  scans has recently been published from our current healthy controls and patients.<sup>11</sup>

**Phase-contrast x-ray micro-computed tomography.** PC- $\mu\text{CT}$  was performed at the Göttingen Instrument for Nano-Imaging with X-Rays (GINIX) end-station, P10 beamline of the PETRA III storage ring at DESY (Hamburg, Germany). The x-ray beam, which is produced by an undulator acting on the 6 GeV storage ring, was set to an energy of 8 keV by a Si (111) monochromator. While the main purpose of the end-station is high-resolution holographic imaging using waveguide, compound optics, and a cone-beam geometry, the images presented in this study have been obtained in the parallel-beam configuration, previously detailed.<sup>14</sup> In brief, the parallel (unfocused)

**Table 1** Subject characteristics

Age, sex, code	Duration (year)	Clinical diagnosis	Histopathological findings	Histopathological diagnosis	NTV/TTV <sup>†</sup> (%)
<b>Controls</b>					
45, M (A)		Control	Normal neurons	Healthy	3.84
54, M (B)		Control	Normal neurons	Healthy	5.27
61, M (C)		Control	Normal neurons	Healthy	5.21
61, M (D)		Control	Normal neurons	Healthy	3.93
82, M (E)		Control	Normal neurons	Healthy	5.26
85, W (F)		Control	Normal neurons	Healthy	2.92
<b>Patients</b>					
27, W (A)	4	Type 1 diabetes/autonomic neuropathy	Vacuolated, apoptotic neurons, chromatolysis	Lymphocytic ganglioneuritis	3.76
27, W (B)	6	Idiopathic dysmotility	Vacuolated neurons, chromatolysis	Degenerative neuropathy	3.47
32, W (C)	2	Drug-induced CIPO	Vacuolated, shrunken, chromatolysis, hyperplasia ICC	Visceral degenerative neuropathy with axon vacuolization, hyperplasia, and vacuolization of ICCs, and hypertrophy of the longitudinal and internal circular muscle layers.	3.76
43, W (D)	3	Idiopathic dysmotility	Amphophilic shrunken neurons, Vacuolated neurons, chromatolysis	Lymphocytic ganglioneuritis with neurodegeneration	2.59
52, W (E)	4	Idiopathic dysmotility	Vacuolated, shrunken neurons, hypoplasia of ICC	Lymphocytic ganglioneuritis	2.67
56, W (F)	50	Ehlers–Danlos	Vacuolated neurons, chromatolysis, hyperplasia ICC	Lymphocytic ganglioneuritis with vacuolar neurodegeneration and hyperplasia of the ICC	2.51

<sup>†</sup>Data from the present x-ray phase-contrast micro-computed tomography examination. All other data was obtained from the medical records. Disease duration assessed in years. “Age” is the age at diagnosis and not actual current age. The letter codes A–F correspond to the codes in Figures 4 and 5.

CIPO, chronic intestinal pseudo-obstruction; ICC, interstitial cells of Cajal; M, man; NTV, neural tissue volume; TTV, total tissue volume; W = woman.

undulator beam was used with opened slits, in combination with continuous tomographic rotation (Micos UPR 160-AIR, PI miCos). The image acquisition system (Optique Peter, France) was based on a 50- $\mu\text{m}$  thick LuAG:Ce scintillator, a 10 $\times$  magnifying microscope objective and a sCMOS sensor (pco.edge, PCO), resulting in an effective pixel size of 0.65  $\mu\text{m}$  and a field of view of  $\sim 1.7 \times 1.4 \text{ mm}^2$  (H  $\times$  W). The acquisition time was set to 35 ms per projection, for a total scan time of about 1.5 min for a full scan (360°) with 1500 projections. Phase retrieval, ring removal, and tomographic reconstruction were performed with in-house reconstruction pipelines.<sup>15</sup>

The field of view was comparable to that of the lab-based overview scans presented in our previous paper,<sup>10</sup> but with a higher image quality and in a fraction of the time. High-resolution holographic scans with the waveguide configuration were also performed on the current cohort, but the high variance of structures in the imaged volumes greatly hindered

segmentation and made a quantification attempt statistically unviable. However, those scans have been studied with a qualitative approach, more akin to standard histological evaluation, in a different publication with detailed description of pathological neuronal changes.<sup>11</sup>

**Image analysis.** The images were filtered with a nonlocal means filter in Amira (Thermo Fisher Scientific, Waltham, Massachusetts, USA), to improve the signal to noise ratio. The neural tissue was then segmented using a combination of the Carving tool in Ilastik<sup>16</sup> and the Magic Wand tool in Amira. This enabled a 3D rendering of the neural tissue structure, which was visualized in Amira. The rest of the tissue was also separated from the paraffin by simple grayscale thresholding. From the segmented data, the ratio of neural tissue volume (NTV) over total tissue volume (TTV), (NTV/TTV), was then calculated. To account for the fact that in some samples the myenteric plexus would move

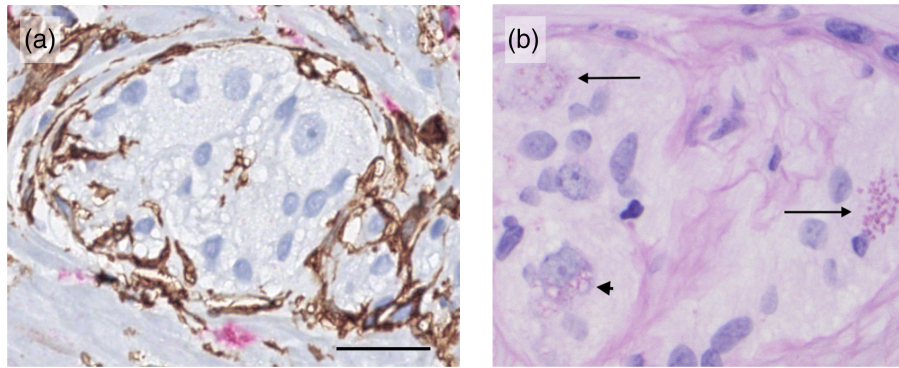


**Figure 1** Histopathology. (a) Normal neurons in healthy control (Control sample B), Myenteric ganglia of ileum. Scale bar: 25  $\mu\text{m}$  (light microscopy; double labeling, CD34/c-Kit; telocytes (TC): brown, interstitial cells of Cajal (ICC): red). (b) Two degenerating neurons from patient (Patient sample A). The cytoplasm of the neuron is filled with diastase-resistant periodic acid-Schiff (PAS)+ lipofuscin granules (arrows). At the arrowhead, vacuoles of the neuron have PAS-D positive rim (light microscopy; PAS-D staining). Panel (a) is reproduced from J Cell Mol Med. 2020;24:3399–3406<sup>12</sup> (CC BY).

outside of the punched volume, but other tissue would continue deeper in the punch, the volume evaluation was only carried out between the first and last transversal slice in which the myenteric plexus was visible. A measurement of the neural tissue thickness was also performed with the Filament tool in Amira, which consists in a skeletonization of the segmented structure and then a distance map measure on the voxels that are part of the skeleton. In practice, this is equivalent to fitting the largest possible spheres along the center line of the segmented structures; the measured diameter of the spheres corresponds to the thickness of the structure in that point.

**Statistical analysis.** The difference in NTV/TTV between controls and patients was calculated with the Mann–Whitney *U* test in the statistical software package SPSS, version 28, data for Windows. Values are given as median (interquartile ranges). A *P*-value <0.05 was considered statistically significant.

All patients had been examined due to clinical indications. The use of the collected samples and clinical data was performed in accordance with the Helsinki declaration and approved by the Regional Ethics Review Board at Lund University (2012/527, 2016/943, 2018/583. Date of approval 16 October 2012, 15 November 2016, 21 June 2018) and the Swedish Biobank Act. Subjects gave their written, informed consent before inclusion in the present study. The scanning was conducted from 25 February to 1 March 2019 in Göttingen and 14–18 September 2019 in Hamburg. Only the corresponding author had access to the code list of the pseudonymized participants.

## Results

### Histopathological findings in light microscopy.

Light microscopy analysis in HE staining showed normal neurons and nerve fibers in all six control samples (Table 1). Immunostaining was performed for clinical diagnosis in the six patients included according to the CIPO protocol, and the histopathological findings were classified as previously defined;<sup>17,18</sup> the results were extracted from the medical records. The histopathological evaluation showed normal number of neurons in

two patients (A, E), although many of them were swollen with or without vacuolation of cytoplasm and/or nucleus. In the other four patients (B, C, D, F), the total number of neurons was reduced, and the ganglia were small, with the same findings of swollen or shrunken, vacuolated neurons. The nerve trunks and/or nerve fibers were thickened and vacuolated in three of them (B, C, D). Chromatolysis was apparent in all cases representing dying neurons, and small granule indicating autophagia were apparent in one patient (A) (Fig. 1). The number of ICC and telocytes was increased in three patients (C, D, F) and reduced in two (B, E). The number of glial cells was increased in one patient (B), and the number of T-lymphocytes was increased in four patients (A, D, E, F). Staining of B-cell lymphoma 2 (Bcl-2) and synaptophysin were absent or reduced in all cases, whereas substance P was reduced in four patients (B, C, E, F) and vasoactive intestinal peptide (VIP) in three patients (D, E, F).

**Volumetric evaluation via PC- $\mu$ CT.** Figure 2 depicts a virtual slice of one of the samples and illustrates the contrast provided by PC- $\mu$ CT. The distinction was clear between the neural components and the surrounding muscle cells and connective tissue. Thus, the ENS could be clearly segmented and visualized in 3D, as described in the Methods section, and the volume of the neural tissue could be determined in all samples. The individual ratio of NTV/TTV is reported in Table 1. The ratio of NTV/TTV between controls and patients was significantly higher in the controls (4.57 [3.61–5.26]%) compared with the patients (3.07 [2.57–3.76]%) (*P* = 0.013) (Fig. 3).

Figures 4 and 5 show the segmented networks in controls and in patients, respectively, filled with spheres to measure the local cross-sectional thickness. The Filament tool in Amira could extract the average diameter of the different segments of the network, as well as the segment length. The thickness distribution for each sample, that is, which percentage of the total network length has which thickness, could then be visualized in histogram plots (Figs 4, 5). For an easier comparison, the *x*-axis of all the histograms covers the same thickness range, between 0 and 130  $\mu\text{m}$  (the largest measured among all samples). The

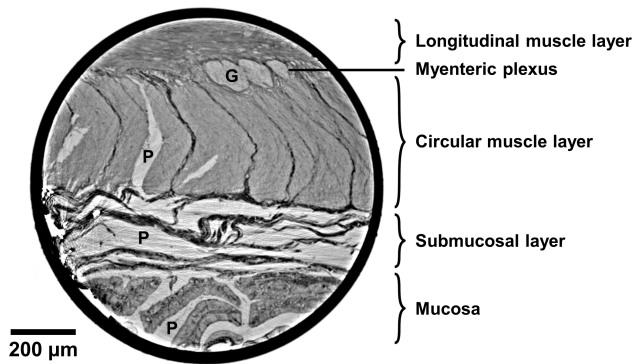


**Figure 2** Example of x-ray phase-contrast micro-computed tomography slice of a sample. The virtual slice is transversal to the Kapton® tube in which the biopsy punch has been inserted. All the different tissue layers are distinguishable and have been labeled on the right side. In the myenteric plexus, a ganglion (G) is visible. The paraffin (P) from the embedding has penetrated in parts of the circular muscle layer, as well as in the submucosal layer and in the mucosa; its contribution has been excluded from the volumetric analysis by means of simple gray-scale thresholding.

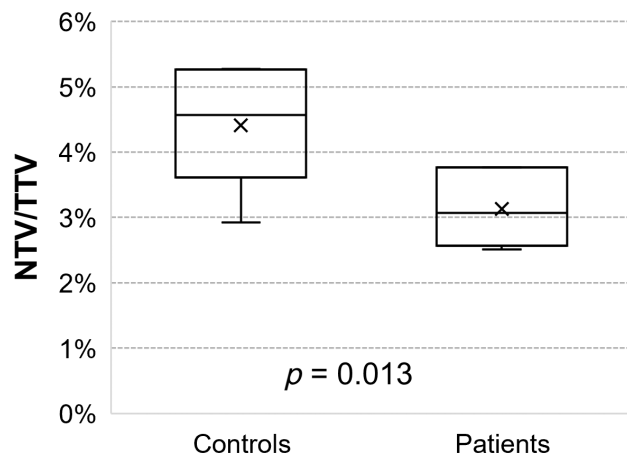


**Figure 3** Box plot comparing neural tissue volume (NTV)/total tissue volume (TTV) in health and disease. The NTV/TTV values for each individual sample are presented in Table 1. The plot shows median (line), mean (cross), interquartile range (box), and min/max (whiskers) of the two populations. The reported *P*-value was obtained by the Mann-Whitney *U* test.

histograms are also color-coded to match the coloring of the spheres, to more easily correlate thickness distribution and spatial location. A variation within the sample could be appreciated from the thickness distributions, which was not reflected in the NTV/TTV numbers.

The spatial organization of both ganglia and fascicles looked normal in both controls and patients. However, the fascicles looked very thin among most of the patients (Fig. 5A, B and D–F), whereas very few fascicles were thin in the control samples (Fig. 4E, F). Among the patients, the patient with the longest

disease duration had the lowest NTV/TTV ratio (2.51%). The individual with an acute debut of CIPO, with a short disease duration, was the patient with the most preserved neural volume (3.76%) (Table 1). The two controls with thinner fascicles (E and F) were the two oldest individuals. In sample F, the network was also quite sparse, resulting in the lowest NTV/TTV among controls (2.92%). In sample E, the fascicles were more numerous, resulting in a much higher NTV/TTV (5.26%), on par with the other controls.

## Discussion

The main finding in the present study was that PC- $\mu$ CT could identify and assess the neural structure and volume of the myenteric plexus in the ileum of both patients with gastrointestinal dysmotility/CIPO and of healthy controls. The method is reproducible and reliable,<sup>19</sup> and when performed on a synchrotron setup, it can potentially analyze many samples in a very short time.

Traditionally, the ENS is studied using light microscopy with immunohistochemical stains of different cells, receptors, and proteins, with the great advantage of being able to selectively identify specific types of cells such as glial cells, ICCs, or telocytes. One of the shortcomings of this time-consuming method is that the influence on receptors and proteins varies between patients, and it has not been possible to identify a uniform pattern in patients with CIPO or other dysmotility.<sup>9</sup> Thus, the usefulness of this extensive staining to diagnose neuropathy is limited. In addition, the paraffin sections have a thickness of 3–5  $\mu$ m, whereas the thickness of the neurons varies between 15 and 40  $\mu$ m.<sup>7</sup> The number of available ganglia in the section is therefore limited, and it is difficult to assess atrophy/hypertrophy and the organization of the ENS. An immunohistochemical method for 3D visualization has been developed, which, however, involves advanced methods for handling and staining of the tissue samples.<sup>20</sup> There is a clear need for more reliable methodology which can examine larger areas and is less user dependent.

To evaluate the usefulness of PC- $\mu$ CT as a novel method to perform more robust 3D analysis, we have used this technique to examine controls and patients with diagnosed enteric neuropathy. The most important findings of this 3D analysis were that the connections between ganglia and trunks could be followed in all imaged samples; thus, the ENS volume could be quantified, and the degree of atrophy or hypertrophy should be possible to evaluate in the future when appropriate reference values for age and sex are obtained. Furthermore, the representativeness of the findings can be strengthened by imaging larger volumes of tissue. A whole paraffin block could be scanned, with the obvious advantages of larger sampled volume, shorter preparation time, and reduced bias in selecting the area.<sup>21</sup> One last significant advantage is that the method does not require any specific type of staining nor specific sample preparation, to the point that it could potentially be performed in fresh samples as well.<sup>22</sup>

Volume and thickness estimations through PC- $\mu$ CT show great promise for the diagnosis of enteric neuropathy; however, they would not entirely replace traditional methods. Theoretically, neuropathy may be present with reduced function in the neurons, although the volume is normal. Even though the

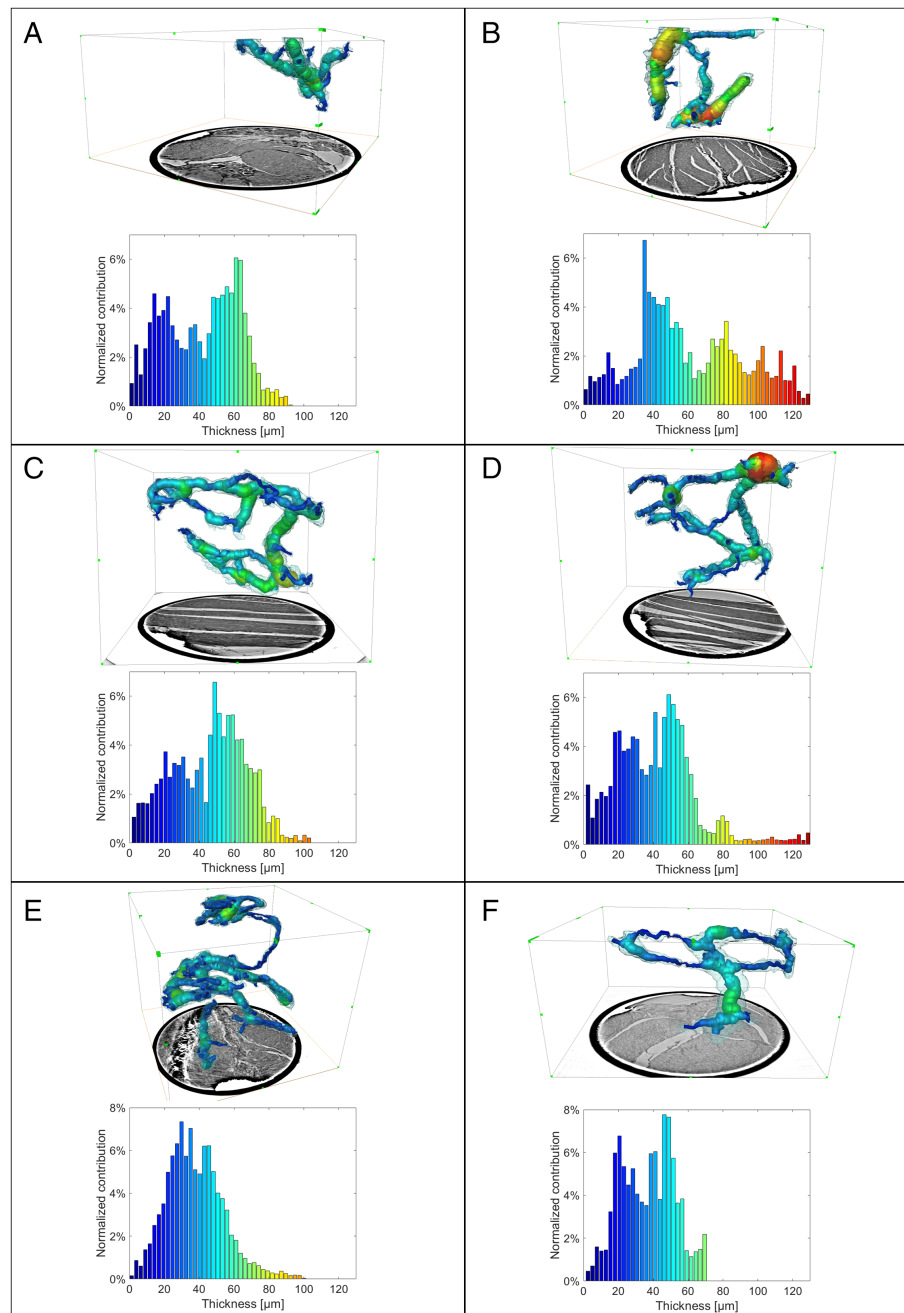


**Figure 4** Volume and thickness analysis in the controls. The letters A–F correspond to the different control sample entries in Table 1. For each sample, a 3D rendering of the neural tissue network is presented in light transparent gray, filled with colored spheres that are color-coded depending on their diameter. As detailed in the [Methods](#) section, each sphere's diameter corresponds to the local thickness estimation. A wireframe box around the rendering informs about the perspective distortion that comes from representing the 3D object as a 2D picture. A virtual slice transversal to the sample, like the one shown in Figure 2, is also added to provide an indication of the size. Below each rendering, a histogram plot of the neural tissue thickness distribution is presented. The x-axis of all the histograms covers the same thickness range, between 0 and 130  $\mu\text{m}$  (the largest measured among all samples). The histograms are also color-coded to match the coloring of the spheres, to better correlate thickness distribution and spatial location.

number of neurons may be reduced as observed in light microscopy, the volume may be preserved due to swollen neurons. On the other hand, some neurons may be shrunken and reduced in size, but the number of neurons may be higher than normal. In

those cases, a histopathological evaluation of high-resolution x-ray scans,<sup>11</sup> or conventional immunohistochemistry, would be required to complete the volume determination, with details of pathological changes in the cells and tissue components.

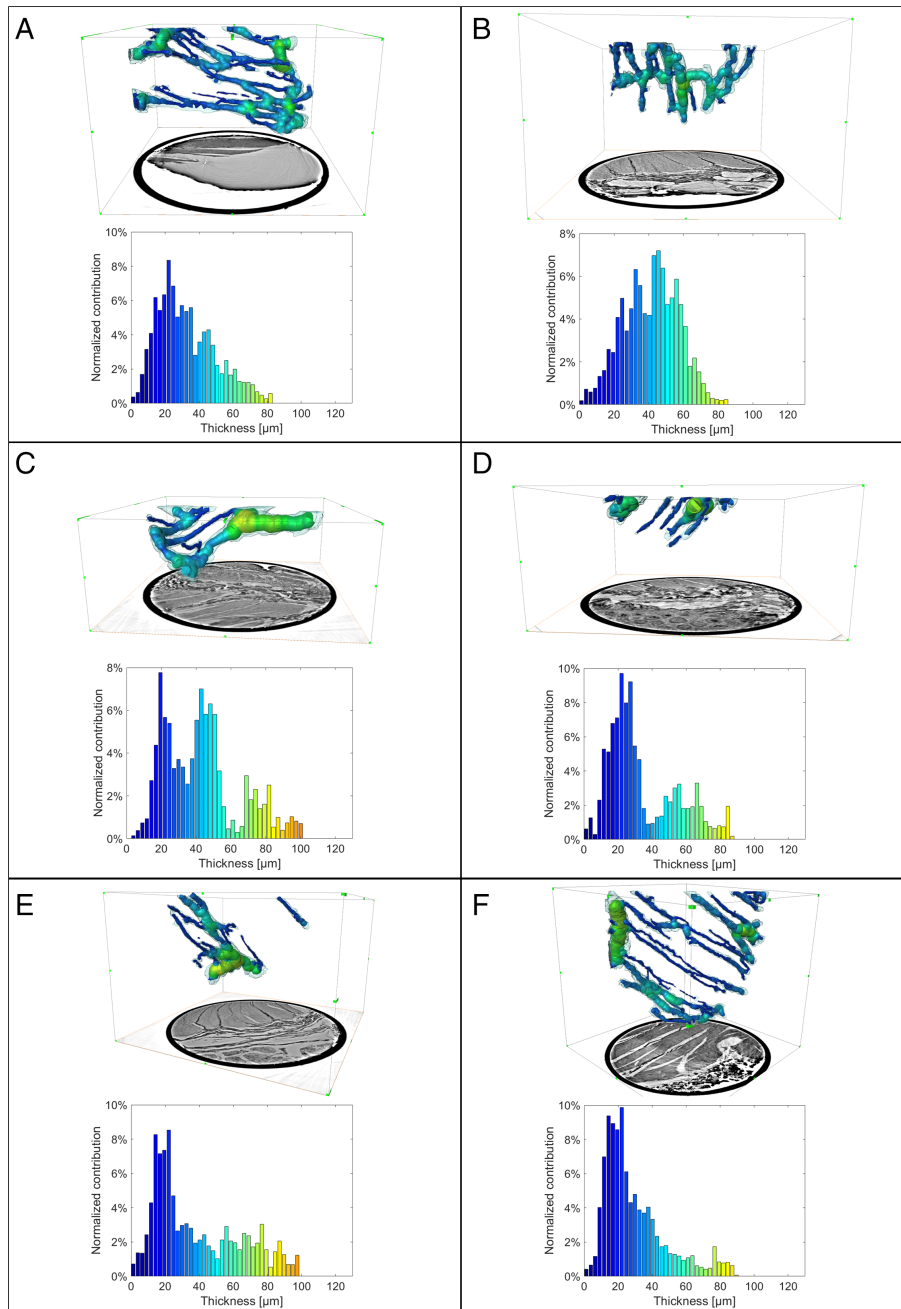


**Figure 5** Volume and thickness analysis in the patients. The letters A–F correspond to the different patient sample entries in Table 1. For each sample, a 3D rendering of the neural tissue network is presented in light transparent gray, filled with colored spheres that are color-coded depending on their diameter. As detailed in [Methods](#) section, each sphere’s diameter corresponds to the local thickness estimation. A wireframe box around the rendering informs about the perspective distortion that comes from representing the 3D object as a 2D picture. A virtual slice transversal to the sample, like the one shown in Figure 2, is also added to provide an indication of the size. Below each rendering, a histogram plot of the neural tissue thickness distribution is presented. The x-axis of all the histograms covers the same thickness range, between 0 and 130 μm (the largest measured among all samples). The histograms are also color-coded to match the coloring of the spheres, to better correlate thickness distribution and spatial location.

One could speculate that the volume is more reduced for longer disease duration, and interestingly, the patient with longest disease duration in this study had the lowest NTV/TTV ratio. In

many cases, however, it is difficult to exactly determine disease onset, because the debut may be slowly progressive. The oldest control (85 years of age) was the one with lowest ratio, which

may be explained by reduced neurons by age.<sup>23</sup> The second oldest control (82 years of age), while having a high NTV/TTV, presented a lower average thickness of the neural structures compared with the younger controls. Nevertheless, the small sample size does not allow to draw any conclusion in this sense at the current stage. The great variation in clinical findings, histopathological findings, and volume of neural tissue emphasizes the importance of larger sample sizes of both controls and patients, to determine reference values for ENS under physiological and pathological conditions, for both sexes and different ages.

Compared with our former methodology publication,<sup>10</sup> which only compared one control and one patient, the present study is a further step in the direction of larger sample sizes. An additional strength is the use of controls from ileum, thus having control samples from the same region as the patient samples. However, the same result remained, with less neural volume in the patients than in the controls. A final very substantial advantage of this study with synchrotron radiation is the fast scan time of ~1.5 min per sample (relative to the ~15 h per sample in our previous study in Peruzzi *et al.*<sup>10</sup> where the volume and thickness evaluations were carried out on laboratory-based setups). Even though the synchrotron setup provided higher speed and better image quality, while also granting the option to perform higher-resolution scans of selected areas, it is important to highlight that studies carried out in a laboratory setting have easier accessibility compared with a synchrotron setting.

The main limitation of the presented technique was the use of punch biopsy of 1 mm diameter. The determination of the NTV is dependent on the extraction of a representative location from the paraffin blocks. However, this restriction on sample diameter was determined by the decision of performing high-resolution cone-beam x-ray nanoCT on the samples (examples of which have been shown in previous publications<sup>10,11</sup>). A study like the one here presented, which only aims to distinguish the neural components from the surrounding tissue, could also be performed with lower resolutions and larger samples. A larger sampled volume would also allow to measure characteristics of other tissue types which might not fit within a 1-mm biopsy punch. For example, as degenerative myopathy may appear secondary to the neuropathy, or may be a primary disorder,<sup>2-4</sup> it might be of interest to measure a reduction in volume of the two muscle layers. Such a measurement was not feasible in this study, as not all the 1-mm samples contained a comparable volume of muscles but would be possible by imaging the full thickness of the muscle layers. To properly assess the degree of atrophy or hypertrophy, more samples will need to be scanned with determination of reference values for both sexes, different ages, and different segments of the gastrointestinal tract under physiological conditions. As several of the CIPO cases are pediatric patients,<sup>24</sup> we would envision a future use of this technique also in a pediatric setting.

In conclusion, PC- $\mu$ CT suggests a reduced volume of the myenteric plexus in the ileum of patients with gastrointestinal dysmotility/CIPO compared with healthy controls. Changes in local cross-sectional thickness were also identified between different subjects, which might hint at differences related to age or disease. The assessment can be performed in an objective, standardized way, to ensure reproducibility and comparison between physiological and pathological conditions. Further evaluation is

needed to examine the role of this method in the diagnosis of enteric neuropathy.

## Acknowledgments

The authors would like to thank the late Béla Veress for his skillful help with the identification of the ENS and for the passionate discussions about the data analysis. The authors also thank Maria Teresa Moreira Jara and Maria Nilsson for technical help. We acknowledge DESY (Hamburg, Germany), a member of the Helmholtz Association HGF, for the provision of experimental facilities. Parts of this research were carried out at PETRA III, and we would like to thank Michael Sprung, Fabian Westermeyer, and Markus Osterhoff for assistance in using the GINIX end-station at the P10 beamline. Beamtime was allocated for proposal I-20190127. The study was presented as an oral poster by Peruzzi N, Eckermann M, Frohn J, Salditt T, Ohlsson B, Bech M, titled "Quantitative evaluation of the enteric nervous system in health and disease via x-ray phase-contrast tomography," at UEGW in Copenhagen, 16–18 October 2023.

## Informed consent

Subjects gave their written, informed consent for publication.

**Data availability statement.** A  $2 \times 2 \times 2$  binned, 8-bit depth version of the PC- $\mu$ CT data used for this study is publicly hosted on the Open Science Framework (OSF) platform at the following link: "<https://osf.io/m9uh8/>." Full size data are available from the corresponding author upon request.

## References

- Furness JB, Callaghan BP, Rivera LR, Cho H-J. The enteric nervous system and gastrointestinal innervation: integrated local and central control. In: Lyte M, Cryan JF (eds). *Microbial Endocrinology: The Microbiota-Gut-Brain Axis in Health and Disease*. New York, NY: Springer, 2014; 39–71.
- Camilleri M, Bharucha AE, Di Lorenzo C *et al.* American neurogastroenterology and motility society consensus statement on intraluminal measurement of gastrointestinal and colonic motility in clinical practice. *Neurogastroenterol. Motil.* 2008; **20**: 1269–82.
- Knowles CH, Giorgio RD, Kapur RP *et al.* The London classification of gastrointestinal neuromuscular pathology: report on behalf of the gastro 2009 international working group. *Gut.* 2010; **59**: 882–7.
- Keller J, Bassotti G, Clarke J *et al.* Advances in the diagnosis and classification of gastric and intestinal motility disorders. *Nat. Rev. Gastroenterol. Hepatol.* 2018; **15**: 291–308.
- Basilisco G, Marchi M, Coletta M. Chronic intestinal pseudo-obstruction in adults: a practical guide to identify patient subgroups that are suitable for more specific treatments. *Neurogastroenterol. Motil.* 2024; **36**: e14715.
- Bertoli D, Mark EB, Liao D *et al.* MRI-based quantification of pancreatic function and motility in subjects with diabetes and gastrointestinal symptoms. *J. Clin. Med.* 2023; **12**: 5968.
- Hitchcock RJ, Pemble MJ, Bishop AE, Spitz L, Polak JM. Quantitative study of the development and maturation of human oesophageal innervation. *J. Anat.* 1992; **180**: 175–83.
- Törnblom H, Lindberg G, Nyberg B, Veress B. Full-thickness biopsy of the jejunum reveals inflammation and enteric neuropathy in irritable bowel syndrome. *Gastroenterology.* 2002; **123**: 1972–9.

- 9 Hammar O, Ohlsson B, Veress B, Alm R, Fredrikson GN, Montgomery A. Depletion of enteric gonadotropin-releasing hormone is found in a few patients suffering from severe gastrointestinal dysmotility. *Scand. J. Gastroenterol.* 2012; **47**: 1165–73.
- 10 Peruzzi N, Veress B, Dahlin LB *et al.* 3D analysis of the myenteric plexus of the human bowel by x-ray phase-contrast tomography – a future method? *Scand. J. Gastroenterol.* 2020; **55**: 1261–7.
- 11 Veress B, Peruzzi N, Eckermann M *et al.* Structure of the myenteric plexus in normal and diseased human ileum analyzed by x-ray virtual histology slices. *World J. Gastroenterol.* 2022; **28**: 3994–4006.
- 12 Veress B, Ohlsson B. Spatial relationship between telocytes, interstitial cells of cajal and the enteric nervous system in the human ileum and colon. *J. Cell. Mol. Med.* 2020; **24**: 3399–406.
- 13 Töpperwien M, van der Meer F, Stadelmann C, Salditt T. Three-dimensional virtual histology of human cerebellum by x-ray phase-contrast tomography. *Proc. Natl. Acad. Sci.* 2018; **115**: 6940–5.
- 14 Frohn J, Pinkert-Leetsch D, Mißbach-Güntner J *et al.* 3D virtual histology of human pancreatic tissue by multiscale phase-contrast x-ray tomography. *J. Synchrotron Radiat.* 2020; **27**: 1707–19.
- 15 Lohse LM, Robisch A-L, Töpperwien M *et al.* A phase-retrieval toolbox for x-ray holography and tomography. *J. Synchrotron Radiat.* 2020; **27**: 852–9.
- 16 Berg S, Kutra D, Kroeger T *et al.* Ilastik: interactive machine learning for (bio)image analysis. *Nat. Methods.* 2019; **16**: 1226–32.
- 17 Ohlsson B, Veress B, Janciauskiene S, Montgomery A, Haglund M, Wallmark A. Chronic intestinal pseudo-obstruction due to busarelin-induced formation of anti-GnRH antibodies. *Gastroenterology.* 2007; **132**: 45–51.
- 18 Lindberg G, Törnblom H, Iwarzon M, Nyberg B, Martin JE, Veress B. Full-thickness biopsy findings in chronic intestinal pseudo-obstruction and enteric dysmotility. *Gut.* 2009; **58**: 1084–90.
- 19 Eckermann M, Schmitzer B, van der Meer F *et al.* Three-dimensional virtual histology of the human hippocampus based on phase-contrast computed tomography. *Proc. Natl. Acad. Sci.* 2021; **118**: e2113835118.
- 20 Graham KD, López SH, Sengupta R *et al.* Robust, 3-dimensional visualization of human colon enteric nervous system without tissue sectioning. *Gastroenterology.* 2020; **158**: 2221–2235.e5.
- 21 Westöö C, Norvik C, Peruzzi N *et al.* Distinct types of plexiform lesions identified by synchrotron-based phase-contrast micro-CT. *Am. J. Physiol. Lung Cell. Mol. Physiol.* 2021; **321**: L17–28.
- 22 Pacilè S, Baran P, Dullin C *et al.* Advantages of breast cancer visualization and characterization using synchrotron radiation phase-contrast tomography. *J. Synchrotron Radiat.* 2018; **25**: 1460–6.
- 23 Hanewinkel R, Drenthen J, van Oijen M, Hofman A, van Doorn PA, Ikram MA. Prevalence of polyneuropathy in the general middle-aged and elderly population. *Neurology.* 2016; **87**: 1892–8.
- 24 Turcotte M-C, Faure C. Pediatric intestinal pseudo-obstruction: progress and challenges. *Front. Pediatr.* 2022; **10**: 837462.